Research Square

Preprints are preliminary reports that have not undergone peer review.
They should not be considered conclusive, used to inform clinical practice,
or referenced by the media as validated information.

Early Mars valley networks require decoupled surface water and groundwater

Eric Hiatt

eric.hiatt@utexas.edu

The University of Texas

Mohammad Afzal Shadab

Princeton University https://orcid.org/0000-0002-0797-5017

Sean Gulick

University of Texas at Austin https://orcid.org/0000-0003-4740-9068

Timothy Goudge

The University of Texas at Austin https://orcid.org/0000-0003-4297-9838

Marc Hesse

University of Texas at Austin https://orcid.org/0000-0002-2532-3274

Physical Sciences - Article

Keywords: Mars, water, climate, groundwater, decoupled surface-subsurface hydrology

Posted Date: August 14th, 2026

DOI: https://doi.org/10.21203/rs.3.rs-10167991/v1

License: This work is licensed under a Creative Commons Attribution 4.0 International License.
Read Full License

Additional Declarations: There is **NO** Competing Interest.

Early Mars valley networks require decoupled surface water and groundwater

Eric Hiatt[1,2,3,4*], Mohammad Afzal Shadab[5,6], Sean P. S. Gulick[1,2,3], Timothy A. Goudge[2,3], Marc A. Hesse[2,3,7]

[1*]University of Texas Institute for Geophysics, The Jackson School of Geosciences, The University of Texas at Austin, 10601 Exploration Way Building 196, Austin, 78758, TX, U.S.A..
[2]The Department of Earth and Planetary Sciences, The Jackson School of Geosciences, The University of Texas at Austin, 2305 Speedway, Austin, 78712, TX, U.S.A..
[3]The Center for Planetary System Habitability, The University of Texas at Austin, 2305 Speedway, Austin, 78712, TX, U.S.A..
[4]Department of Earth, Environmental, and Planetary Sciences, Washington University in St. Louis, One Brookings Drive, St. Louis, 63130, MO, U.S.A..
[5]Department of Civil and Environmental Engineering, Princeton University, 54 Olden Street, Princeton, 08544, NJ, U.S.A..
[6]Integrated Ground Water Modeling Center, High Meadows Environmental Institute, Princeton University, 11 Ivy Lane, Princeton, 08544, NJ, U.S.A..
[7]Oden Institute for Computational Engineering and Sciences, The University of Texas at Austin, 01 E 24th St, Austin, 78712, TX, U.S.A..

*Corresponding author(s). E-mail(s): eric.hiatt@utexas.edu;
Contributing authors: mashadab@princeton.edu; sean@ig.utexas.edu; tgoudge@jsg.utexas.edu; mhesse@jsg.utexas.edu;

Abstract

The ancient surface of Mars records both runoff carved valley networks and evidence for groundwater activity [1, 2], yet how much surface water reached regional aquifers remains uncertain. We use valley network elevations to constrain

groundwater table height, comparing them with transient simulations that alternate between recharge and quiescence. Across 365 simulations spanning recharge intensity, duration, and spacing, the groundwater response is controlled by a single parameter: time averaged recharge over mean hydraulic conductivity. Compatibility with valley network incision, which requires groundwater to remain below valley floors, is met only when regional recharge is a small fraction of precipitation estimates. Within a 100 Myr valley network forming interval, only low recharge fractions permit many runoff episodes, whereas the terrestrial median recharge fraction of 22% [3] would limit cumulative wet time to only a few of the longest episodes. A single $\geq\mathbf{10^5}$ yr warm event, the minimum duration in coupled climate photochemical models [4], would exceed this entire budget. We infer that valley network forming runoff was at most weakly coupled to regional groundwater recharge. A weakly coupled surface and subsurface water cycle suggests caution is merited in inter-comparisons of the hydrology implied by surface and subsurface geologic and geomorphic observations on Mars.

Keywords: Mars, water, climate, groundwater, decoupled surface-subsurface hydrology

Branching networks of river valleys incised into the southern highlands are among the most direct evidence that liquid water once flowed across the surface of Mars, and they anchor reconstructions of its early climate [1, 2]. Valley networks record the geomorphic work done by runoff, but not the efficiency with which that runoff recharged regional groundwater [e.g., 5–8]. Widespread valley networks formed before the late Noachian to the early Hesperian at ∼3.7 Ga [1], and these networks are widely distributed, locally incised to kilometer depths, and weakly integrated over tens of thousands of kilometers [9–13] (Fig. 1).

The climatic conditions that produced the valley networks remain debated, with proposed end members ranging from sustained rainfall and surface runoff to colder scenarios in which snow or ice accumulated and melted only episodically [2, 14]. These end members also imply different hydrological architectures. Warm and wet scenarios likely suggest vertical integration between runoff, infiltration, and groundwater recharge, whereas cold and icy scenarios favor a more horizontally stratified system in which communication between surface water and regional subsurface is limited by a shallow cryosphere across the planet [15, 16].

The valley networks record the routing of surface water across topographic catchments, but do not record the efficiency of recharge to regional aquifers. In terrestrial systems, the interactions between groundwater and surface water typically set the regional base level, which influences the elevation to which rivers can persistently incise [17–19]. Preserved valley network elevations can therefore constrain groundwater table height during runoff producing climates. Due to slow diffusion rates in the regional aquifer, groundwater heights can retain information regarding the integration of previous hydrological activity [13]. The elevation of the groundwater table responds to the cumulative magnitude, partitioning, and time between the recharge events and is filtered by the hydraulic conductivity of the aquifer and the drainage distances [20–22]. To promote widespread valley incision, we expect groundwater to remain consistently

below valley network floors. Alternatively, if efficient recharge raised groundwater above these elevations, we would expect widespread seepage and groundwater driven deposition, as observed in Arabia Terra [23]. We test this prediction with transient numerical simulations of the Martian hydrologic system in response to periods of groundwater recharge and subsequent quiescence, or intra-recharge periods. Our simulations span a range of recharge intensity, recharge duration, and intra-recharge interval. Ultimately, we use these data to address the question: is the runoff required to form the valley networks compatible with a vertically integrated hydrosphere on early Mars?

Model evaluation

We use transient groundwater simulations to test how regional aquifers would respond if the runoff that produced valley network formation was accompanied by groundwater recharge. Each simulation assumes a repeating hydrological cycle, illustrated in Fig. 2a. During recharge intervals, groundwater is recharged across low- to mid-latitude highlands, and the northern lowland, Argyre, and Hellas basins are set to a highstand shoreline. During intervening intra-recharge intervals, recharge ceases, the shoreline elevation shifts to a lowstand shoreline, and the aquifer drains. The highstand and lowstand are the maximum and minimum basin water levels of the recharge cycle. By varying the recharge rate, the duration of the recharge intervals, and the duration of the intervening intra-recharge periods, the simulations explore how combinations of these parameters impact groundwater table elevations. Recharge is therefore explicitly time variable: it is applied as a square wave in time ($\Gamma(t)$; Methods), active at constant intensity during recharge intervals and zero during intra-recharge intervals (Fig. 2a).

We then compare each simulated groundwater surface with the mapped valley networks using the analysis metric shown in Fig. 2b. The average elevation of the valley networks in each grid cell, z_{VN}, is treated as the elevation that groundwater must remain below to sustain valley incision. The model calculates the groundwater table elevation, z_{GW}, in the same cell. We define the groundwater margin

$$\Delta z = z_{\mathrm{GW}} - z_{\mathrm{VN}}, \tag{1}$$

so that $\Delta z < 0$ indicates groundwater below the valley network floor and $\Delta z > 0$ indicates groundwater at or above it. Because not all cells contain the same density of valley network terrain, we weigh each cell by its mapped valley network density and define F_{VN} as the valley network density weighted fraction of terrain where $\Delta z > 0$, i.e., essentially fraction of valley network terrain at the same elevation as the groundwater table. This provides a single scalar summary for each simulation that can be compared across the full parameter sweep.

Transient groundwater responses

To evaluate these model simulations, we compute Δz in each grid cell and summarize each simulation by F_{VN} (Fig. 2). Across the full parameter sweep of recharge intensity, recharge duration, and intra-recharge interval (365 simulations), z_{GW} increases systematically with the ratio of time averaged recharge over depth averaged hydraulic

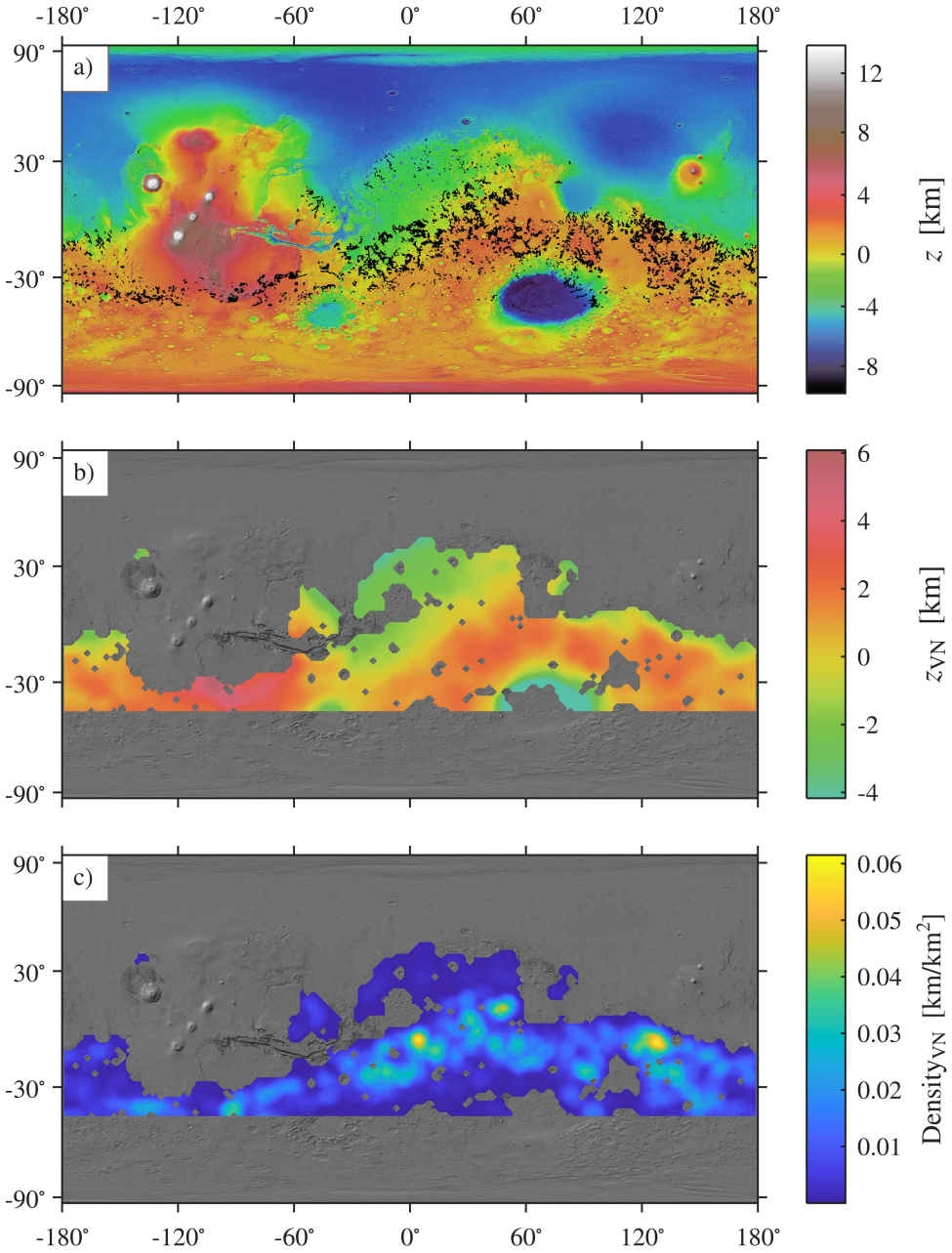


Fig. 1 Global distribution, elevation, and density of Late Noachian to Early Hesperian Martian valley networks. a) Mars Orbiter Laser Altimeter (MOLA) topography [24] overlain by mapped valley networks (black) [11, 25]. Late Noachian to Early Hesperian age valley networks, between 45°N and 45°S, are retained to minimize inclusion of networks modified by glacial processes. **b)** Valley network elevation, z_{VN}, relative to the Martian datum, defined as half the valley depth below the adjacent rim crest. All elevations in this manuscript are measured from the datum and are positive in the upward direction. z_{VN} values are then binned and averaged to the model resolution of $2° \times 2°$ per pixel. **c)** Valley network density, ρ_{VN}, expressed as mapped valley length per unit area (km/km^2). Background for **b** and **c** is a MOLA-derived hillshade.

conductivity, $\bar{r}/\bar{K}$ (see Methods). This ratio was previously identified as the primary control on groundwater elevation in steady state simulations [26]. Here, it denotes the recharge averaged over the imposed sinusoidal geometry and the recharge cycle, divided by the vertically averaged aquifer conductivity. In Fig. 3a-c, the recharge duration and intra-recharge interval are fixed at 5 kyr and 1 Ma, so the increase in $\bar{r}/\bar{K}$ reflects increases in recharge rate during episodes of recharge. At low $\bar{r}/\bar{K}$ (1.5×10^{-5}), $\Delta z < 0$ across most valley network terrain. At intermediate $\bar{r}/\bar{K}$ (4.4×10^{-5}), positive Δz expands across the main valley network belt. At high $\bar{r}/\bar{K}$ (9.3×10^{-5}), positive Δz covers the majority of valley network terrain.

The temporal evolution illustrated in Fig. 3d, and animated in Supplementary Video 1, shows that, after a short adjustment interval, each simulation approaches a periodic steady state imposed by the recharge periodicity. F_{VN} increases systematically from the low to high $\bar{r}/\bar{K}$ scenarios, from roughly one quarter to more than four fifths of weighted valley network terrain. Once a periodic steady state is established, the oscillation amplitude of F_{VN} remains modest relative to the separation between cases, so throughout the remaining manuscript we present distinctions among simulations based on the mean F_{VN} rather than the maximum or minimum.

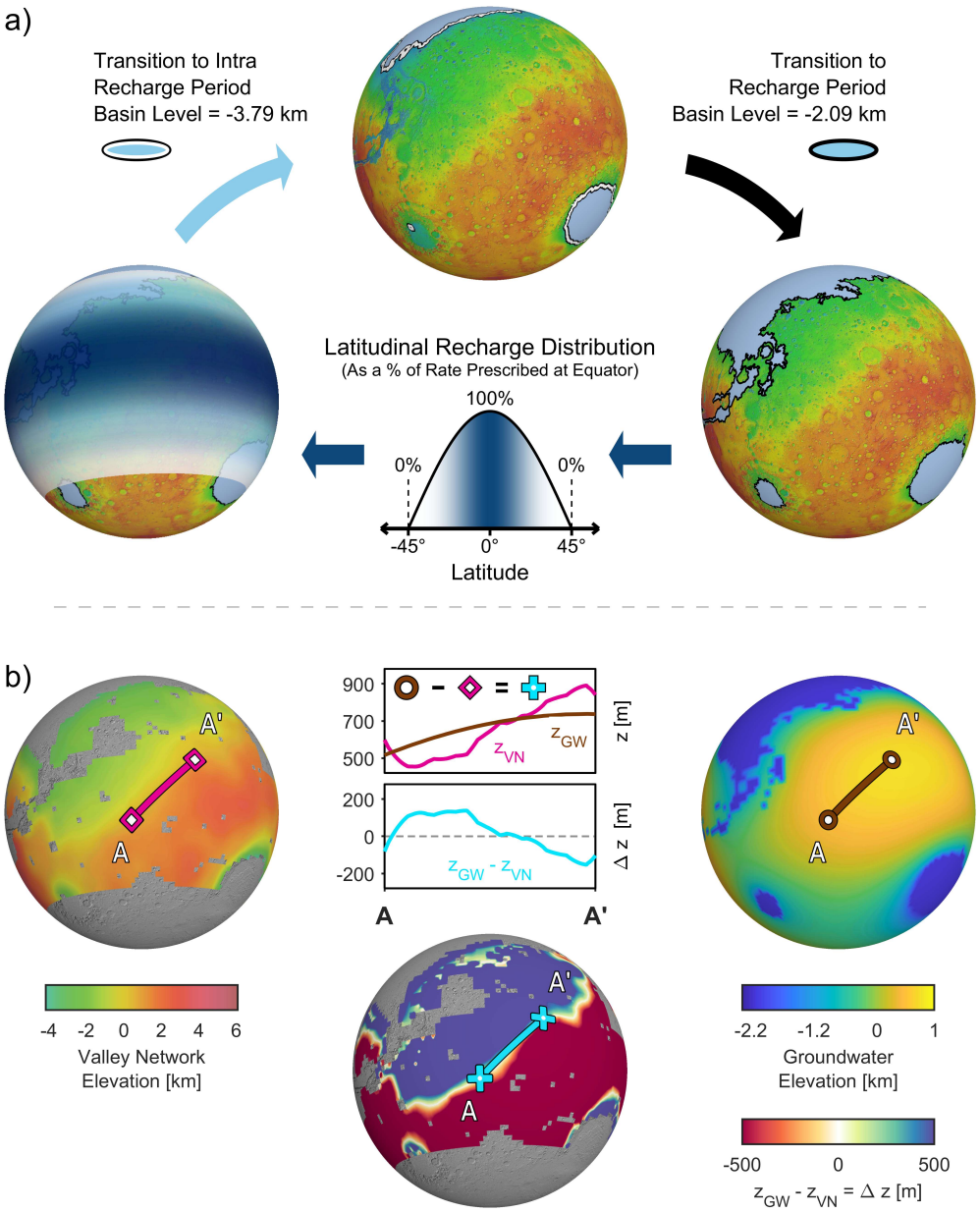
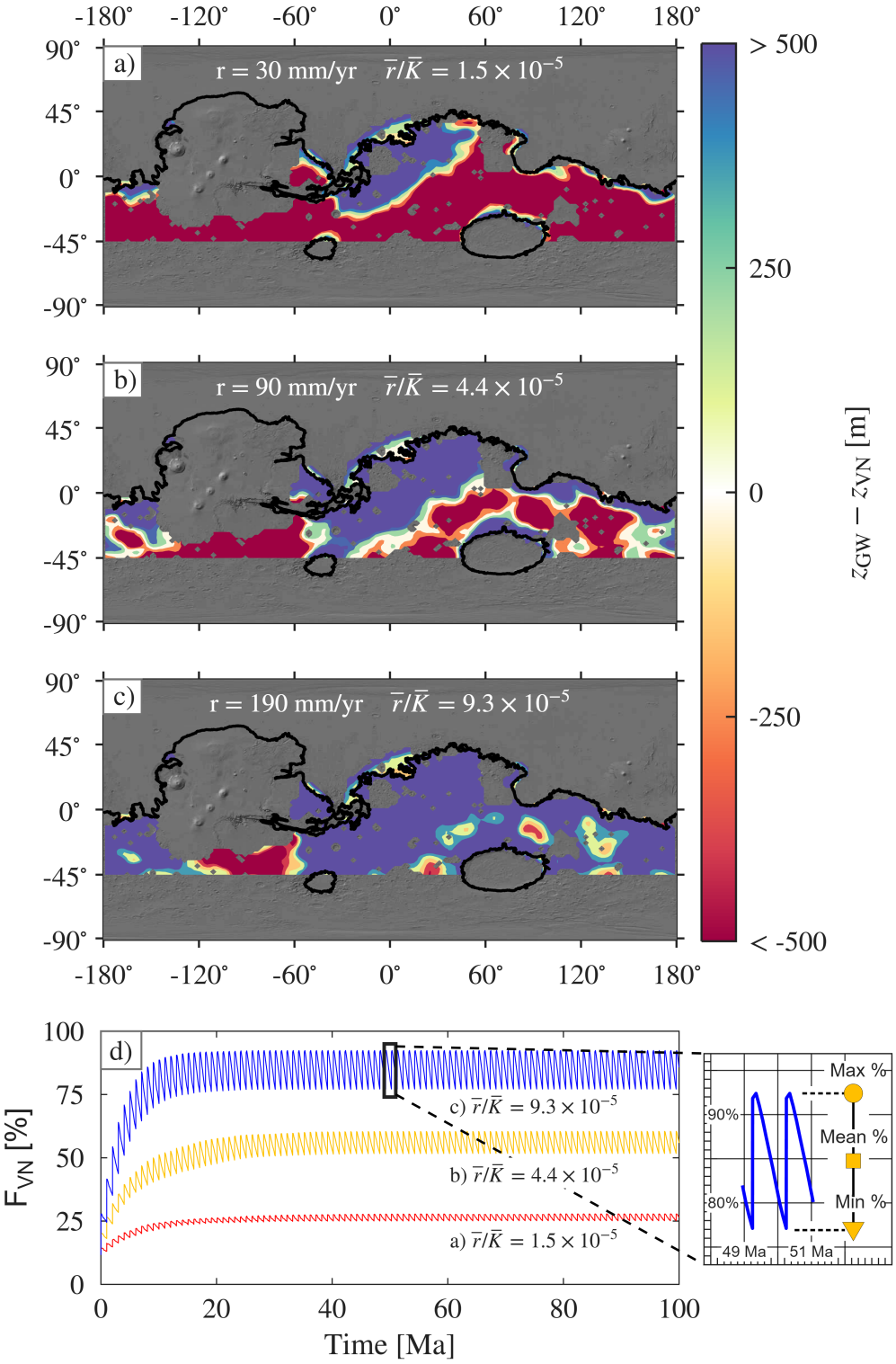


Fig. 2 Conceptual framework and analysis metric used to evaluate transient groundwater simulations. a) Recharge cycle. During the intra-recharge period, basin shorelines are set to −3.79 km. During the recharge period, shorelines transgress to −2.09 km and recharge is applied between 45°S and 45°N with a cosine distribution, normalized at the equator. **b)** Illustration of the analysis metric. Valley network elevations, z_{VN}, are defined as half the valley depth below the adjacent rim crest, then averaged to the model grid. For each cell we compute $\Delta z = z_{\mathrm{GW}} - z_{\mathrm{VN}}$, where z_{GW} is the modeled groundwater table elevation. Positive Δz indicates groundwater above representative valley network elevations, and negative Δz indicates groundwater below. Cells are weighted by mapped valley network density, and each simulation is summarized by F_{VN}, the weighted fraction of valley network terrain where $\Delta z > 0$. Valley network data are modified from Goudge et al. (2024) [12].



7

Fig. 3 Representative transient groundwater responses. a) to **c)** Groundwater margin $\Delta z = z_{GW} - z_{VN}$ for 5 kyr recharge and 1 Ma intra-recharge simulations. Maps are taken at the first recharge timestep after the preceding intra-recharge interval, once each simulation had reached pseudo-periodic steady state. This corresponds to the beginning of a recharge episode, near the minimum value marked in the panel d inset. Recharge rates and time averaged $\bar{r}/\bar{K}$ are labeled in each panel. Black contours mark the −2.09 km recharge period basin level. **d)** F_{VN}, the valley network weighted terrain fraction where $\Delta z > 0$. The inset shows periodic steady state cycles with minimum, mean, and maximum values. Mean values are used in Fig. 4a. The temporal evolution corresponding to this figure is animated in Supplementary Video 1.

Groundwater dynamics controlled by $\bar{r}/\bar{K}$

Despite the complexity of the model, we find that F_{VN} is controlled by a single parameter $\bar{r}/\bar{K}$. All 365 simulations together show a highly consistent, nonlinear relationship between F_{VN} and time averaged $\bar{r}/\bar{K}$ (Fig. 4a), despite spanning orders of magnitude in recharge intensity and recharge and intra-recharge episode durations. For $\bar{r}/\bar{K} < 10^{-5}$, F_{VN} is minimal. Near $\bar{r}/\bar{K} \sim 10^{-5}$, F_{VN} increases rapidly. At higher $\bar{r}/\bar{K}$, flooding of valley network terrain is pervasive, with F_{VN} reaching 90% in some cases. This emergent relationship, a property of the ensemble rather than of any individual simulation, defines which transient scenarios are compatible with valley network locations and elevations.

In this model, groundwater behavior is characterized by $\bar{r}/\bar{K}$. The threshold near 10^{-5} signifies when groundwater in our model remains below valley network elevations across most of the southern highlands. This shows that the groundwater response is not individually controlled by the intensity of the recharge, the duration of the event, and the recurrence, but by their combined effect due to the long groundwater response time scale. This finding gives a direct way to compare model results with previous hydrological estimates that constrain fluxes, durations, and/or intermittency of surface runoff and groundwater recharge.

Valley network runoff and regional recharge

To compare valley network forming runoff with the groundwater compatibility threshold, we convert published runoff estimates into nominal time averaged $\bar{r}/\bar{K}$ values rather than treating the reported runoff as direct recharge. These estimates come from two classes of studies: geomorphic or channel hydraulic reconstructions of runoff intensity required to incise valley networks [27, 28], and climate modeling studies that report runoff, precipitation, and/or erosion rates for early Mars scenarios constrained by valley network formation [29, 30]. In our comparison with Hoke et al. [28], we use only their conservative inner channel runoff estimates. For each reported runoff intensity q_{run}, we partition total water input between surface runoff and recharge using a recharge fraction f_r, then apply an intermittency of $I = 5\%$ to obtain a nominal $\bar{r}/\bar{K}$ (Supplementary). Table 1 therefore asks how much surface-to-groundwater coupling can exist before the modeled groundwater table rises above valley network elevations. Even at $f_r = 1\%$, the lowest converted values, 3.8×10^{-5}–2.2×10^{-4}, are already above the compatibility threshold $\sim 10^{-5}$, and the 5% and 22% recharge cases increase the mismatch by factors of ~ 5 and ~ 28, respectively, the latter fraction corresponding to the terrestrial median [3]. Only the lowest runoff values with a 1% recharge partitioning approach $\bar{r}/\bar{K}$ of 10^{-5}; the remainder require a partition of runoff into recharge at levels $\ll$1%.

The mismatch between estimates of precipitation and limits on recharge is not study specific. Taking a wide range of runoff or water availability estimates of 10^2 to 10^5 mm/yr [28–36], combined with a 1% infiltration partitioning and 5% intermittency, results in calculated $\bar{r}/\bar{K}$ values of $\sim 1.5 \times 10^{-5}$ to 1.5×10^{-2}, at, or significantly above the 10^{-5} threshold, implying F_{VN} approaching 90%, indicating flooding across large portions of valley network terrain. This behavior contradicts the observed valley

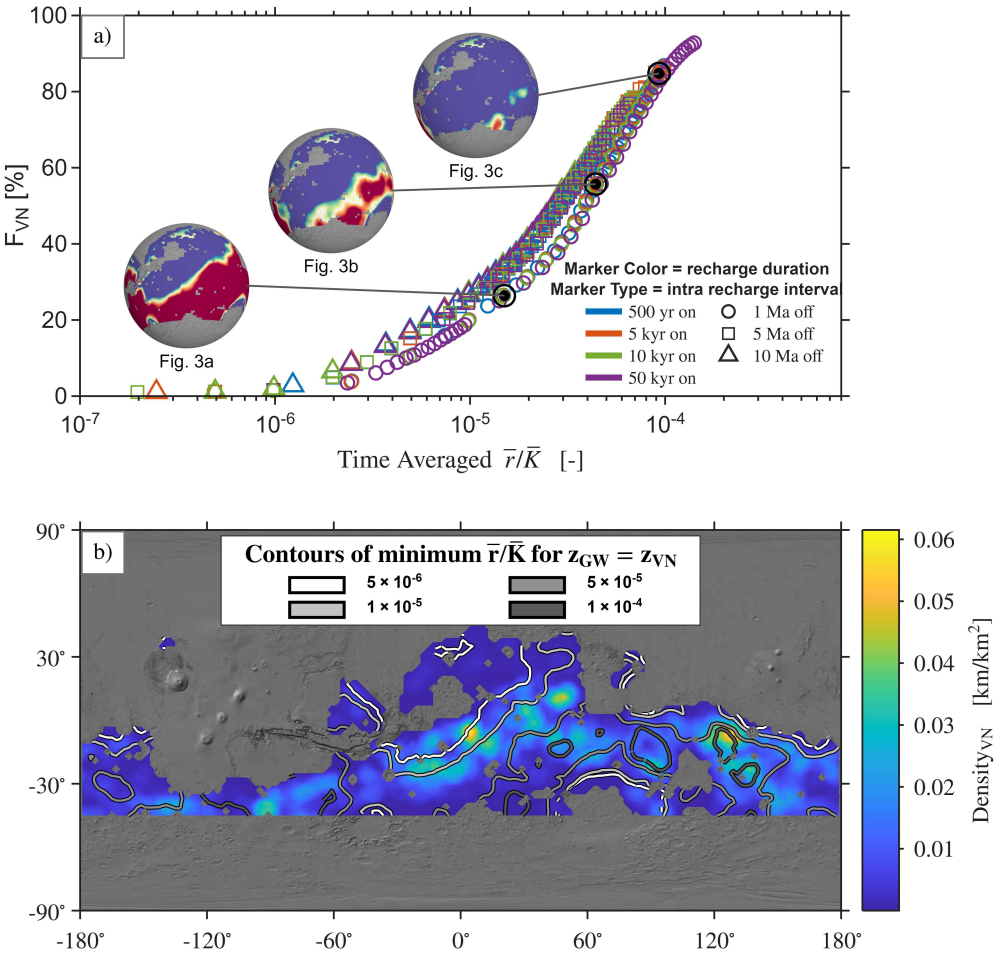


Fig. 4 Time averaged $\bar{r}/\bar{K}$ organizes the full transient parameter sweep. a) Results from 365 simulations showing the nonlinear relationship between F_{VN} and time averaged $\bar{r}/\bar{K}$. Symbol color denotes recharge duration and type denotes intra-recharge interval. Representative cases from Fig. 3 are highlighted. **b)** Valley network density from Fig. 1c overlain by contours of the minimum time averaged $\bar{r}/\bar{K}$ required for $\Delta z = 0$ (groundwater reaching valley network elevations). These contours identify where groundwater compatibility with observed valley networks is first exceeded.

incision, which would require groundwater to remain regionally below valley floors for sustained periods during episodes of surface runoff. Large areas with $\Delta z > 0$ would have also generated seepage and groundwater-related deposition across valley network terrain, for which there is no geologic evidence (outside of Arabia Terra) [23].

Therefore, we conclude that the discrepancy between previous runoff estimates and our model-derived threshold for $\bar{r}/\bar{K}$ implies that surface runoff and regional groundwater recharge were at most weakly coupled. If even a modest fraction of the precipitation infiltrated to recharge the regional aquifer, the high elevation of the groundwater table would have suppressed the continued incision of valley networks,

and instead favored widespread deposition. Effective recharge therefore must have been limited to $< 1\%$ of total precipitation for all scenarios considered here.

Table 1 Runoff estimates based on valley network morphology converted to effective $\bar{r}/\bar{K}$ assuming intermittency $I = 5\%$ and recharge fractions of 1%, 5%, and 22%. Values listed for Hoke et al. (2011) only include the conservative inner channel-based estimates.

Study	Runoff (mm day^{-1})	$\bar{r}/\bar{K}$ (1%)	$\bar{r}/\bar{K}$ (5%)	$\bar{r}/\bar{K}$ (22%)
Hoke et al. (2011)	4–50	$(0.22–2.7) \times 10^{-3}$	$(1.1–14) \times 10^{-3}$	$(0.61–7.6) \times 10^{-2}$
Irwin et al. (2005)	1–60	$(0.055–3.3) \times 10^{-3}$	$(0.29–17) \times 10^{-3}$	$(0.15–9.2) \times 10^{-2}$
von Paris et al. (2015)	1.5–10.6	$(0.82–5.8) \times 10^{-4}$	$(0.43–3.0) \times 10^{-3}$	$(0.23–1.6) \times 10^{-2}$
Ramirez et al. (2020)	0.7–9.69	$(0.38–5.3) \times 10^{-4}$	$(0.20–2.8) \times 10^{-3}$	$(0.11–1.5) \times 10^{-2}$

Intermittency and storage as restrictive alternatives

Low intermittency provides one way to reduce the time averaged recharge recorded by the regional aquifer, and is not excluded by existing constraints. Hydrologic analysis of coupled lake systems suggests breaching runoff episodes commonly lasted 10^2–10^4 yr, with model dependent limits extending to 10^5 yr [37]. A valley network forming interval of order 10^8 yr could therefore accommodate many short runoff episodes separated by long intra-recharge intervals. Such constraints are not inconsistent with previous estimates, but they are restrictive. The climate must produce repeated, geologically short runoff episodes while keeping cumulative recharge to the regional aquifer small.

The allowed number of long-duration episodes falls rapidly as runoff intensity or recharge fraction increases. With 0.1% of precipitation reaching the regional aquifer, the $\bar{r}/\bar{K}$ threshold permits $\sim 10^2$–10^3 episodes of 10 kyr duration at 1–10 mm day^{-1}. At 22% recharge it permits only $\sim$3 such episodes at 1 mm day^{-1}, and fewer than one at 10 mm day^{-1}. These budgets scale linearly with the formation interval, and $T_{\rm form} = 100$ Myr is the maximum permitted by crater statistics [38], so any shorter interval only tightens the constraint. Independent climate considerations sharpen it further. Coupled photochemical-climate modeling limits warmth driven by crustal hydration to a cumulative ~ 2–4×10^7 yr, delivered as $\sim$1–100 events each lasting $\geq 10^5$ yr [4]. This floor, set by atmospheric H_2 buildup and escape, coincides with the $\lesssim 10^5$ yr ceiling on individual runoff episodes from coupled lake systems [37]. Climate physics and lake hydrology thus converge on $\sim 10^5$ yr as the characteristic scale of the longest individual wet events. A single event of this duration with sustained runoff would exceed the entire groundwater compatible wet time budget at the terrestrial recharge fraction by a factor of $\sim$3–30, and accommodating runoff across the full $\sim 4 \times 10^7$ yr of warm time would require recharge fractions $\lesssim 0.02\%$ even at 1 mm day^{-1}. Intermittency therefore remains viable only when solutions are pushed toward low recharge fractions and short runoff episodes. It does not allow for a strongly coupled system under higher runoff or terrestrial like recharge. See the Supplementary for detailed calculations.

Excess subsurface storage, whereby the deep groundwater system is under filled, is a similarly restrictive alternative. Published estimates suggest the crust above a deep aquifer could store tens of meters GEL (Global Equivalent Layer) of water, with deeper pore space filling for inventories of order 100 m GEL [39, 40]. These are comparable to the lower end of proposed ocean inventories, so storage cannot be dismissed on volume alone [41–44]. Our model already includes large surface reservoirs implicit in the shoreline boundary conditions. The imposed highstand to lowstand transition corresponds to $\sim$ 200 m GEL across all three basins with moving shorelines, the northern lowlands (including Utopia and Isidis), Argyre, and Hellas, so their surface water is represented rather than treated as additional subsurface capacity. Large basin forming impacts are nonetheless sometimes invoked as a source of the pore volume this scenario requires. The Argyre and Hellas basins lie in the southern highlands, where their impacts created deep, fractured crust that could host substantial pore space and may also have compartmentalized regional groundwater flow rather than feeding a single integrated aquifer [45]. This source is less helpful than it first appears. Both basins are interpreted to have held large standing bodies of water at various times [46–48], and a filled basin in hydraulic contact with the regional aquifer feeds the water table through its own floor rather than draining it. Such a basin lowers the regional table only transiently, while the deep reservoir it created is still filling, and thereafter acts as a persistent recharge source unless it is hydraulically disconnected from the regional system. The basins therefore supply net storage only in the same decoupled configuration the data already favor. The efficiency of infiltration sharpens this constraint. Vertical recharge through the Martian crust reaches the deep aquifer in decades to centuries [39], so where surface and subsurface are hydraulically connected, infiltration is not rate limiting and available pore space fills as water is supplied rather than remaining open across geologic time. A basin reservoir that stayed unfilled through the $\sim 10^8$ yr valley network forming era could therefore persist only if it were largely isolated from the surface, which is itself the decoupling our results infer. Storage may therefore help in favorable cases, but only if substantial pore volume was available, initially unsaturated, and able to retain infiltrated water without rapidly transmitting it to the regional aquifer.

This creates a tradeoff between available surface and subsurface water. If storage is effective, infiltrated water leaves the active surface cycle until returned to the surface or atmosphere. Sustaining repeated runoff, lake filling, and incision then requires recycling stored water, a challenge on a planet without plate tectonics, or adding new water. Alternatively, water rock reactions may remove it permanently, as crustal hydration and oxidation sequester water in hydrated minerals [44, 49, 50], a process also implicated in generating episodic warm climates through H_2 release [4]. Either way, storage is not a free sink. It sequesters water away from continued runoff or participates in the regional groundwater response. Moreover, widespread pre-valley network crater degradation likely involved some surface water [e.g., 2, 51–53], making it unlikely the valley network forming era began with an empty, globally available pore volume.

Critically, neither alternative rescues a coupled hydrosphere, because each is itself a form of decoupling. Low recharge fractions, highly intermittent runoff, and large

unfilled storage all produce the same signature, namely the regional water table remaining below valley network floors while surface runoff is vigorous, and differ only in why the table stays low. Intermittency decouples the surface and subsurface in time, whereas storage decouples them by interception. The inference of a weakly coupled surface and regional groundwater system is therefore robust to these alternatives rather than undermined by them. Both intermittency and storage thus remain plausible only under highly favorable assumptions about event timing, available pore space, and water recycling. The simpler interpretation is that a large proportion of the precipitation responsible for valley incision did not recharge the regional aquifer during valley network formation.

Implications for the hydrologic structure of early Mars

Our results lead us to conclude that early Mars did not operate as the vertically integrated surface and subsurface hydrologic system as most terrestrial systems. When precipitation sufficient to incise valley networks occurred, only a small fraction recharged the regional groundwater system, so the surface hydrosphere was only weakly connected to the deep subsurface. Valley networks then record the routing of surface runoff across topography, while groundwater records a filtered, time averaged recharge signal. The decoupling permits widespread incision without raising regional groundwater to valley network elevations and the subsequent production of widespread deposits similar to those in Arabia Terra.

Our results constrain the degree of vertical coupling but not the mechanism that maintained it. The barrier to recharge could be a conventional aquiclude of subsurface clays formed by the water rock alteration noted above [49, 50], or a frozen confining layer, a cryospheric analogue we term a cryoclude, in which a planet wide cryosphere isolates surface water from a deeper aquifer [54]. Decoupling also requires no barrier at all in the open system storage case, where unfilled pore space intercepts infiltration before it reaches the regional water table. Our results cannot distinguish among these mechanisms, but this does not weaken the central inference, because each independently keeps the regional water table below valley network floors during vigorous surface runoff.

This reframes how surface and subsurface records should be jointly interpreted. Geomorphic evidence of vigorous surface runoff and geochemical and hydrologic evidence of limited groundwater activity need not be contradictory. In a weakly coupled Mars they can be interpreted as complementary records of reservoirs that communicated inefficiently. The recharge fraction itself becomes a quantitative climate diagnostic, linking the intensity and intermittency of surface runoff to the magnitude of the groundwater response. A weakly coupled surface and subsurface water cycle suggests caution is merited in inter-comparisons of the hydrology implied by surface and subsurface geologic and geomorphic observations on Mars.

Methods

Mars data products

The model is informed with gridded MOLA topography that is down sampled (via averaging) to the 2° per pixel model resolution [55] projected into spherical coordinates to match the model's geometric discretization. The distributions, densities, and elevations of the valley networks were obtained from Goudge et al. (2024) [12] and also down sampled to the same grid resolution. Each grid cell was assigned a representative valley network elevation as the rim crest elevation minus half the local valley depth for each mapped segment in the grid, then averaged across the grid cell. Valley network density was assigned to each cell as the mean of the per-network densities of all mapped networks whose center coordinates fall within the cell, where each per-network density is its total mapped length divided by the fixed 1.96×10^{11} m^2 (250 km radius) search area of the source dataset [12]. Each cell is weighted by this density, and each simulation is summarized by F_{VN}, the valley network density weighted fraction of terrain where $\Delta z > 0$, evaluated at each simulation timestep. Formally,

$$F_{\mathrm{VN}} = \frac{\sum_i \rho_{\mathrm{VN},i}\, \mathcal{H}(\Delta z_i)}{\sum_i \rho_{\mathrm{VN},i}}, \tag{2}$$

where the sums run over all grid cells i containing mapped valley networks, $\rho_{\mathrm{VN},i}$ is the valley network density (Fig. 1c), Δz_i is the groundwater margin in cell i, and $\mathcal{H}$ is the Heaviside step function ($\mathcal{H} = 1$ for $\Delta z_i > 0$ and 0 otherwise). The valley networks lie within 45° of the equator, where grid cell area varies by about a factor of 1.4. Weighting each cell by its latitude dependent area in addition to its mapped density changes F_{VN} by less than one percentage point, so the metric is insensitive to this choice.

The two shorelines were based on the works of Parker et al. (1989) and Carr and Head (2003) [41, 56]. These shorelines were chosen to maintain consistency with previous work [26] and represent an illustrative high and low stand during recharge versus intra-recharge periods, with unknown forcing. The same highstand and lowstand elevations are imposed on the Argyre and Hellas basins as on the northern lowlands. The volume of water removed between the high and low stand is $\sim$ 200 m GEL and roughly equivalent to the estimated volume of water contained in the Noachian aged polar ice caps [33].

The imposed shorelines require transient standing water in the northern lowlands and southern basins, so the simulations implicitly assume contemporaneous oceans or seas during recharge intervals. The specific shoreline elevation has only a second order effect on the modeled groundwater surface [26], and the presence or absence of an ocean is likewise not a first order effect. An ocean sets the base level, and a lower base level lengthens the groundwater flow paths. Because head gradients in the aquifer diffuse slowly, at a rate set by the hydraulic conductivity, these longer paths allow groundwater to back up and seep rather than drain freely. This is apparent in similar transient groundwater models that lack standing bodies of water and reach equilibrium at lower recharge than presented here [22, 23]. Our shoreline treatment

is therefore conservative, and removing the ocean would only strengthen the inferred decoupling.

Groundwater model

We model groundwater flow in the southern highlands of Mars as a transient aquifer, following previous studies [23, 54, 57]. The governing equation for groundwater head, h, is given by

$$\frac{\phi_0}{m+1}\frac{\partial h^{m+1}}{\partial t} - K_0 \nabla \cdot \left[\frac{h^{n+1}}{n+1}\nabla h\right] = r\,\chi(\theta,\theta_r)\Gamma(t). \tag{3}$$

where K_0 is the hydraulic conductivity coefficient, r is the nominal recharge rate prescribed at the equator, and $\chi(\theta,\theta_r)$ is a function defining the latitudinal extent and weighting of the recharge rate as $\chi(\theta,\theta_r) = \cos(\pi|\theta|/(2\theta_r))$ for $|\theta| < \theta_r$ and $\chi(\theta,\theta_r) = 0$ otherwise, where θ is the latitude. Here θ_r is equatorial band of precipitation that is chosen to be 45°. We assume a vertically heterogeneous hydraulic conductivity using the equation $K = K_0 z^n$ and porosity $\phi = \phi_0 z^m$, with z being the elevation from the bedrock and m and n being the power law coefficients. Compared with the data from the continental crust, their value is $m = 2.54$ and $n = 7.62$, as derived in [39, 58]. The function $\Gamma(t)$, cycles through the user prescribed intervals of time where the aquifer experiences recharge ($\Gamma(t) = 1$) as well as intra-recharge intervals ($\Gamma(t) = 0$).

The aquifer extends from a base elevation of -9 km relative to the Mars datum, consistent with previous studies. We solve the governing equation numerically on a spherical shell. The equation is non-dimensionalized and discretized using a conservative finite-difference scheme on a tensor-product grid, following standard operator-based approaches [59]. The same approach has been successfully applied to validate the model and investigate steady Martian aquifer dynamics, and this work maintains the ability to account for the effects of large standing bodies of water [26]. The resulting nonlinear system is solved using a Newton–Raphson method at each time step.

The model is initialized with the steady state solution of Hiatt et al. [26], whose best-fit equatorial recharge of 0.035 mm yr^{-1} corresponds, after the cosine latitudinal weighting $\chi(\theta,\theta_r)$ is averaged over the recharging highlands, to a spatially averaged $\bar{r}/\bar{K}$ of 3.5×10^{-6}. The transient model employs several techniques to allow for a variable step to resolve arbitrarily short recharge durations while maintaining computational tractability during extended intra-recharge periods. Recharge time scales are subdivided by ten time steps. After a recharge interval, the shoreline is moved to the -3790 m contour line and water table elevations in each reactivated cell is set to topography. The following time step is set to machine precision so that model values are implemented but not held for a full time step. The machine precision time step is subtracted from the subdivided recharge interval time step and after the second time step following the transition, the time step proceeds as the nominal value.

Vertically averaged hydraulic conductivity

The groundwater simulations are formulated using the Dupuit Boussinesq approximation, in which horizontal groundwater flow is governed by the vertically integrated transmissivity of the saturated aquifer. Because hydraulic conductivity is expected to decrease with depth in the Martian megaregolith, we define a vertically averaged hydraulic conductivity, $\bar{K}$, that represents the effective conductivity of the modeled aquifer column. This value is used to nondimensionalize the area- and time averaged recharge rate, $\bar{r}$, through the ratio $\bar{r}/\bar{K}$.

We describe depth below the surface by z, where

$$z = 0 \tag{4}$$

at the surface and

$$z = z_b \tag{5}$$

at the impermeable base of the aquifer. The aquifer thickness is taken to be

$$z_b = 10 \text{ km}. \tag{6}$$

The depth-dependent hydraulic conductivity is represented by a power law decay,

$$K(z) = K_0 \left(1 - \frac{z}{z_b}\right)^n, \tag{7}$$

where K_0 is the near surface hydraulic conductivity and n is the conductivity decay exponent. This form allows the conductivity to decrease continuously with depth and to approach zero at the impermeable base of the aquifer.

The exponent n is related to the assumed porosity–permeability relationship [60]. We first write porosity as

$$\phi(z) = \phi_0 \left(1 - \frac{z}{z_b}\right)^m, \tag{8}$$

where ϕ_0 is the surface porosity and m is the porosity decay exponent. Following the depth-dependent parameterization used in the model, m is obtained by matching this power law form to an exponential porosity decay with e-folding depth z_c,

$$m = \frac{z_b}{2 z_c \ln 2}. \tag{9}$$

For

$$z_b = 10 \text{ km} \tag{10}$$

and

$$z_c = 2.84 \text{ km}, \tag{11}$$

this gives

$$m = 2.54. \tag{12}$$

The permeability is then related to porosity through a power law relationship,

$$k(z) = k_0 \left(1 - \frac{z}{z_b}\right)^n, \tag{13}$$

where p is the porosity–permeability exponent, i.e., $k(\phi) = k_0 \phi^p$. We use

$$p = 3.00, \tag{14}$$

so that the hydraulic conductivity decay exponent is

$$n = mp. \tag{15}$$

With $p = 3.00$ and $m = 2.54$,

$$n = 7.62. \tag{16}$$

Permeability is converted to hydraulic conductivity using

$$K(z) = \frac{k(z)\rho_w g_{\text{Mars}}}{\mu}, \tag{17}$$

where ρ_w is the density of water, g_{Mars} is Martian gravitational acceleration, and μ is the dynamic viscosity of water. We use

$$\rho_w = 1000 \text{ kg m}^{-3}, \tag{18}$$

$$g_{\text{Mars}} = 3.7 \text{ m s}^{-2}, \tag{19}$$

and

$$\mu = 10^{-3} \text{ Pa s}. \tag{20}$$

For a fully saturated aquifer, the vertically averaged hydraulic conductivity is

$$\bar{K} = \frac{1}{z_b} \int_0^{z_b} K(z)\, dz. \tag{21}$$

Substituting equation 7 into equation 21 gives

$$\bar{K} = \frac{1}{z_b} \int_0^{z_b} K_0 \left(1 - \frac{z}{z_b}\right)^n dz. \tag{22}$$

Evaluating the integral yields

$$\bar{K} = \frac{K_0}{n+1}. \tag{23}$$

Thus $\bar{K}$ is not the near surface conductivity, but the depth average of the conductivity profile over the full aquifer thickness.

In the transient simulations and in the literature comparisons, we use

$$\bar{K} = 3.37 \text{ m yr}^{-1} \tag{24}$$

as the representative vertically averaged conductivity of the modeled aquifer. In SI units, this is

$$\bar{K} = \frac{3.37}{365.25 \times 24 \times 3600} = 1.07 \times 10^{-7} \text{ m s}^{-1}. \tag{25}$$

We therefore use $\bar{K} = 10^{-7}$ m s^{-1} to represent the bulk conductivity of the modeled 10 km aquifer column rather than the conductivity of the shallowest regolith alone.

Supplementary information. Supplementary Information accompanies this paper, containing the full aquifer model derivation, numerical methods, and Tables S1–S3.

Acknowledgments. This is University of Texas Institute for Geophysics Contribution #XXXX and Center for Planetary Systems Habitability Contribution #XXXX. T.A.G. acknowledges support from the CIFAR Earth 4D program.

Declarations

Funding. E.H. was supported by a Graduate Student Fellowship from the University of Texas Institute for Geophysics, a Summer Excellence Fellowship from the University of Texas Graduate School, and Student Support Grants from the University of Texas Center for Planetary Systems Habitability. M.A.H. was supported by [NASA program, grant 80NSSC–XXXXX]. M.A.S. acknowledges support from Princeton University's Future Faculty in Physical Sciences Fellowship.

Conflict of interest. The authors declare no competing interests.

Ethics approval and consent to participate. Not applicable.

Consent for publication. Not applicable.

Data availability. MOLA topography is available from the NASA Planetary Data System [55]. The valley network dataset is from Goudge et al. [12]. Gridded model inputs, outputs of all 365 simulations, and source data for Figs. 1–4 will be archived at [Zenodo / Texas Data Repository DOI] upon acceptance.

Materials availability. Not applicable.

Code availability. The transient groundwater model and analysis scripts (MATLAB) will be made available at [GitHub URL] and archived at [Zenodo DOI] upon acceptance.

Author contribution. E.H.: conceptualization, methodology, software, simulations, formal analysis, visualization, writing, original draft. M.A.S.: numerical methods, software, writing and editing. S.P.G.: supervision, funding acquisition, writing and editing. T.A.G.: valley network data, geomorphic interpretation, writing and editing. M.A.H.: conceptualization, methodology, supervision, writing and editing.

References

[1] Fassett, C.I., Head III, J.W.: The timing of martian valley network activity: Constraints from buffered crater counting. Icarus **195**(1), 61–89 (2008)

[2] Craddock, R.A., Howard, A.D.: The case for rainfall on a warm, wet early mars. Journal of Geophysical Research: Planets **107**(E11), 21–1 (2002)

[3] McMahon, P.B., Plummer, L.N., Böhlke, J.K., Shapiro, S.D., Hinkle, S.R.: A comparison of recharge rates in aquifers of the United States based on groundwater-age data. Hydrogeology Journal **19**(4), 779–800 (2011) https://doi.org/10.1007/s10040-011-0722-5

[4] Adams, D., Scheucher, M., Hu, R., Ehlmann, B.L., Thomas, T.B., Wordsworth, R., Scheller, E., Lillis, R., Smith, K., Rauer, H., Yung, Y.L.: Episodic warm climates on early Mars primed by crustal hydration. Nature Geoscience **18**, 133–139 (2025) https://doi.org/10.1038/s41561-024-01626-8

[5] Fassett, C.I., Head, J.W.: Sequence and timing of conditions on early mars. Icarus **211**(2), 1204–1214 (2011)

[6] Ehlmann, B.L., Berger, G., Mangold, N., Michalski, J.R., Catling, D.C., Ruff, S.W., Chassefière, E., Niles, P.B., Chevrier, V., Poulet, F.: Geochemical consequences of widespread clay mineral formation in mars' ancient crust. Space Science Reviews **174**(1), 329–364 (2013)

[7] Kite, E.S.: Geologic constraints on early Mars climate. Space Science Reviews **215**, 10 (2019) https://doi.org/10.1007/s11214-018-0575-5

[8] Kite, E.S., Conway, S.: Geological evidence for multiple climate transitions on early mars. Nature Geoscience **17**(1), 10–19 (2024)

[9] Howard, A.D., Moore, J.M., Irwin III, R.P.: An intense terminal epoch of widespread fluvial activity on early mars: 1. valley network incision and associated deposits. Journal of Geophysical Research: Planets **110**(E12) (2005)

[10] Irwin III, R.P., Howard, A.D., Craddock, R.A.: Fluvial valley networks on Mars. In: Rice, S.P., Roy, A.G., Rhoads, B.L. (eds.) River Confluences, Tributaries and the Fluvial Network, pp. 419–451. John Wiley & Sons, Chichester (2008)

[11] Hynek, B.M., Beach, M., Hoke, M.R.: Updated global map of martian valley networks and implications for climate and hydrologic processes. Journal of Geophysical Research: Planets **115**(E9) (2010)

[12] Goudge, T.A., Morgan, A.M., Stucky de Quay, G., Fassett, C.I.: Spatial patterns of valley network erosion on early Mars. Icarus **421**, 116224 (2024) https://doi.org/10.1016/j.icarus.2024.116224

[13] Ferguson, G., Cuthbert, M.O., Jasechko, S., Manga, M., McDonnell, J.J., McIntosh, J.C., Noyes, C.E., Sherwood Lollar, B., Taylor, R.G.: Renewability of fossil groundwaters affected by present-day climate conditions. Nature Geoscience, 1–5 (2026)

[14] Wordsworth, R.D., Kerber, L., Pierrehumbert, R.T., Forget, F., Head, J.W.: Comparison of "warm and wet" and "cold and icy" scenarios for early Mars in a 3-D climate model. Journal of Geophysical Research: Planets **120**(6), 1201–1219 (2015) https://doi.org/10.1002/2015JE004787

[15] Head, J.W., Marchant, D.R.: The climate history of early mars: insights from the antarctic mcmurdo dry valleys hydrologic system. Antarctic Science **26**(6), 774–800 (2014)

[16] Kite, E.S., Melwani Daswani, M.: Geochemistry constrains global hydrology on Early Mars. Earth and Planetary Science Letters **524** (2019) https://doi.org/10.1016/j.epsl.2019.115718

[17] Leopold, L.B., Bull, W.B.: Base level, aggradation, and grade. Proceedings of the American Philosophical Society **123**(3), 168–202 (1979)

[18] Winter, T.C.: Ground Water and Surface Water: a Single Resource. Diane Publishing, Darby, PA (2000)

[19] Sophocleous, M.: Interactions between groundwater and surface water: the state of the science. Hydrogeology journal **10**, 52–67 (2002)

[20] Freeze, R.A., Witherspoon, P.A.: Theoretical analysis of regional groundwater flow: 1. analytical and numerical solutions to the mathematical model. Water Resources Research **2**(4), 641–656 (1966)

[21] Berkowitz, B., Zehe, E.: Surface water and groundwater: unifying conceptualization and quantification of the two "water worlds". Hydrology and Earth System Sciences **24**(4), 1831–1858 (2020)

[22] Andrews-Hanna, J.C., Lewis, K.W.: Early Mars hydrology: 2. Hydrological evolution in the Noachian and Hesperian epochs. Journal of Geophysical Research: Planets **116**(E2), 02007 (2011) https://doi.org/10.1029/2010JE003709

[23] Andrews-Hanna, J.C., Zuber, M.T., Arvidson, R.E., Wiseman, S.M.: Early Mars hydrology: Meridiani playa deposits and the sedimentary record of Arabia Terra. Journal of Geophysical Research: Planets **115**(E6), 06002 (2010) https://doi.org/10.1029/2009JE003485

[24] Smith, D.E., Zuber, M.T., Solomon, S.C., Phillips, R.J., Head, J.W., Garvin, J.B., Banerdt, W.B., Muhleman, D.O., Pettengill, G.H., Neumann, G.A., *et al.*: The global topography of mars and implications for surface evolution. science

284(5419), 1495–1503 (1999)

[25] Goudge, T.A., Morgan, A.M., Stucky de Quay, G., Fassett, C.I.: The importance of lake breach floods for valley incision on early Mars. Nature **597**(7878), 645–649 (2021) https://doi.org/10.1038/s41586-021-03860-1

[26] Hiatt, E., Shadab, M.A., Gulick, S.P., Goudge, T.A., Hesse, M.A.: Limited recharge of the southern highlands aquifer on early mars. Icarus **408**, 115774 (2024)

[27] Irwin, R.P.I., Craddock, R.A., Howard, A.D.: Interior channels in martian valley networks: Discharge and runoff production. Geology **33**(6), 489–492 (2005) https://doi.org/10.1130/G21333.1

[28] Hoke, M.R., Hynek, B.M., Tucker, G.E.: Formation timescales of large martian valley networks. Earth and Planetary Science Letters **312**(1-2), 1–12 (2011)

[29] von Paris, P., Petau, A., Grenfell, J.L., Hauber, E., Breuer, D., Jaumann, R., Rauer, H., Tirsch, D.: Estimating precipitation on early mars using a radiative-convective model of the atmosphere and comparison with inferred runoff from geomorphology. Planetary and Space Science **105**, 133–147 (2015) https://doi.org/10.1016/j.pss.2014.11.018

[30] Ramirez, R.M., Craddock, R.A., Usui, T.: Climate simulations of early mars with estimated precipitation, runoff, and erosion rates. Journal of Geophysical Research: Planets **125**(3), 2019–006160 (2020)

[31] Soto, A., Richardson, M., Newman, C.: Global constraints on rainfall on ancient mars: Oceans, lakes, and valley networks. In: 41st Annual Lunar and Planetary Science Conference, p. 2397 (2010)

[32] Kite, E.S., Lucas, A., Fassett, C.I.: Pacing early Mars river activity: Embedded craters in the Aeolis Dorsa region imply river activity spanned $\geq$(1–20) Myr. Icarus **225**(1), 850–855 (2013)

[33] Scanlon, K., Head, J.: The dorsa argentea formation: Synthesis of glacial features and history of late noachian-early hesperian martian climate change.(2014) 45th lunar and planetary science conference. LPI Contribution (1777), 1477 (2014)

[34] Fastook, J.L., Head, J.W.: Glaciation in the late noachian icy highlands: Ice accumulation, distribution, flow rates, basal melting, and top-down melting rates and patterns. Planetary and Space Science **106**, 82–98 (2015)

[35] Steakley, K., Murphy, J., Kahre, M., Haberle, R., Kling, A.: Testing the impact heating hypothesis for early mars with a 3-d global climate model. Icarus **330**, 169–188 (2019)

[36] Guzewich, S.D., Way, M.J., Aleinov, I., Wolf, E.T., Del Genio, A., Wordsworth, R., Tsigaridis, K.: 3d simulations of the early martian hydrological cycle mediated by a h2-co2 greenhouse. Journal of Geophysical Research: Planets **126**(7), 2021–006825 (2021)

[37] Stucky de Quay, G., Goudge, T.A., Kite, E.S., Fassett, C.I., Guzewich, S.D.: Limits on runoff episode duration for early Mars: Integrating lake hydrology and climate models. Geophysical Research Letters **48**(15), 2021–093523 (2021) https://doi.org/10.1029/2021GL093523

[38] Morgan, A.M.: New maximum constraints on the era of martian valley network formation. Earth and Planetary Science Letters **626**, 118509 (2024) https://doi.org/10.1016/j.epsl.2023.118509

[39] Shadab, M.A., Hiatt, E., Bahia, R.S., Bohacek, E.V., Steinmann, V., Hesse, M.A.: Infiltration dynamics on early mars: Geomorphic, climatic, and water storage implications. Geophysical Research Letters **52**(8), 2024–111939 (2025)

[40] Squyres, S.W., Clifford, S., Kuz'min, R., Zimbelman, J.R., Costard, F.: Ice in the martian regolith. Mars, 523–554 (1992)

[41] Carr, M.H., Head, J.W.: Oceans on Mars: An assessment of the observational evidence and possible fate. Journal of Geophysical Research E: Planets **108**(5), 1–28 (2003) https://doi.org/10.1029/2002je001963

[42] Clifford, S., Parker, T.: The evolution of the martian hydrosphere: Implications for the fate of a primordial ocean and the current state of the northern plains. Icarus **154**(1), 40–79 (2001)

[43] Fairén, A.G.: A cold and wet mars. Icarus **208**(1), 165–175 (2010)

[44] Scheller, E.L., Ehlmann, B.L., Hu, R., Adams, D.J., Yung, Y.L.: Long-term drying of Mars by sequestration of ocean-scale volumes of water in the crust. Science **7717**(March), 7717 (2021) https://doi.org/10.1126/science.abc7717

[45] Harrison, K.P., Grimm, R.E.: Regionally compartmented groundwater flow on mars. Journal of Geophysical Research: Planets **114**(E4) (2009)

[46] Moore, J.M., Wilhelms, D.E.: Hellas as a possible site of ancient ice-covered lakes on Mars. Icarus **154**(2), 258–276 (2001) https://doi.org/10.1006/icar.2001.6736

[47] Wilson, S.A., Moore, J.M., Howard, A.D., Wilhelms, D.E.: Evidence for Ancient Lakes in the Hellas Region, pp. 195–222. Elsevier B.V., ??? (2010). https://doi.org/10.1016/B978-0-444-52854-4.00007-6 . http://dx.doi.org/10.1016/B978-0-444-52854-4.00007-6

[48] Parker, T., Clifford, S., Banerdt, W.: Argyre planitia and the mars global

hydrologic cycle. In: Lunar and Planetary Science Conference, p. 2033 (2000)

[49] Tutolo, B.M., Tosca, N.J.: Observational constraints on the process and products of Martian serpentinization. Science Advances **9**(5), 8472 (2023) https://doi.org/10.1126/sciadv.add8472

[50] Tosca, N.J., Tice, M.M., Hurowitz, J.A., *et al.*: In situ evidence for serpentinization within the Máaz formation, Jezero crater, Mars. Science Advances **11**(27), 8793 (2025) https://doi.org/10.1126/sciadv.adr8793

[51] Forsberg-Taylor, N.K., Howard, A.D., Craddock, R.A.: Crater degradation in the martian highlands: Morphometric analysis of the sinus sabaeus region and simulation modeling suggest fluvial processes. Journal of Geophysical Research: Planets **109**(E5) (2004)

[52] Mangold, N., Adeli, S., Conway, S., Ansan, V., Langlais, B.: A chronology of early mars climatic evolution from impact crater degradation. Journal of Geophysical Research: Planets **117**(E4) (2012)

[53] Matsubara, Y., Howard, A.D., Irwin III, R.P.: Constraints on the noachian paleoclimate of the martian highlands from landscape evolution modeling. Journal of Geophysical Research: Planets **123**(11), 2958–2979 (2018)

[54] Clifford, S.: A model for the hydrologic and climatic behavior of water on Mars. Journal of Geophysical Research **98**(E6), 10973–11016 (1993) https://doi.org/10.1029/93je00225

[55] Smith, D.E., Zuber, M.T., Frey, H.V., Garvin, J.B., Head, J.W., Muhleman, D.O., Pettengill, G.H., Phillips, R.J., Solomon, S.C., Zwally, H.J., *et al.*: Mars orbiter laser altimeter: Experiment summary after the first year of global mapping of mars. Journal of Geophysical Research: Planets **106**(E10), 23689–23722 (2001)

[56] Parker, T., Saunders, S., Schneeberger, D.: Transitional morphology in west deuteronilus mensae, mars: Implications for modification of the lowland/upland boundary. Icarus **82**(1), 111–145 (1989)

[57] Hanna, J.C., Phillips, R.J.: Hydrological modeling of the Martian crust with application to the pressurization of aquifers. Journal of Geophysical Research: Planets **110**(E1), 01004 (2005) https://doi.org/10.1029/2004JE002330

[58] Shadab, M.A., Hiatt, E., Hesse, M.: Investigating groundwater dynamics and residence times on early mars using unconfined aquifer model with vertical heterogeneity. LPI Contributions, 1736 (2023)

[59] LeVeque, R.J.: Numerical Methods for Conservation Laws, 2nd edn. Birkhäuser Verlag, Basel (1992)

[60] Manning, C.E., Ingebritsen, S.E.: Permeability of the continental crust: Implications of geothermal data and metamorphic systems. Reviews of Geophysics **37**(1), 127–150 (1999)

Supplementary Files

This is a list of supplementary files associated with this preprint. Click to download.

- HiattetalSupplementaryInformation.pdf
- HiattetalSupplementaryVideo1.mp4